

ULRR

Promotion of mefenamic acid nucleation by a surfactant additive, docusate sodium

Item Type	Article
Authors	Bodnár, Katalin;Hudson, Sarah P.;Rasmuson, Åke C.
Citation	Crystal Growth and Design;19 (2), pp. 591-603
Publisher	American Chemical Society
Download date	2026-05-13 00:40:13
Item License	https://creativecommons.org/licenses/by-nc-sa/1.0/
Link to Item	https://hdl.handle.net/10344/7564

Promotion of Mefenamic acid Nucleation by a Surfactant Additive, Docusate Sodium

Katalin Bodnár, Sarah P. Hudson, and Åke C. Rasmuson

Cryst. Growth Des., **Just Accepted Manuscript** • DOI: 10.1021/acs.cgd.8b00995 • Publication Date (Web): 18 Dec 2018

Downloaded from <http://pubs.acs.org> on January 2, 2019

Just Accepted

“Just Accepted” manuscripts have been peer-reviewed and accepted for publication. They are posted online prior to technical editing, formatting for publication and author proofing. The American Chemical Society provides “Just Accepted” as a service to the research community to expedite the dissemination of scientific material as soon as possible after acceptance. “Just Accepted” manuscripts appear in full in PDF format accompanied by an HTML abstract. “Just Accepted” manuscripts have been fully peer reviewed, but should not be considered the official version of record. They are citable by the Digital Object Identifier (DOI®). “Just Accepted” is an optional service offered to authors. Therefore, the “Just Accepted” Web site may not include all articles that will be published in the journal. After a manuscript is technically edited and formatted, it will be removed from the “Just Accepted” Web site and published as an ASAP article. Note that technical editing may introduce minor changes to the manuscript text and/or graphics which could affect content, and all legal disclaimers and ethical guidelines that apply to the journal pertain. ACS cannot be held responsible for errors or consequences arising from the use of information contained in these “Just Accepted” manuscripts.



Promotion of Mefenamic acid Nucleation by a Surfactant Additive, Docusate Sodium

*Katalin Bodnár, Sarah P. Hudson, Åke C. Rasmuson**

Synthesis and Solid State Pharmaceutical Centre, Department of Chemical Sciences,
Bernal Institute, University of Limerick, Limerick V94 T9PX, Ireland

* *E-mail:* Ake.Rasmuson@ul.ie

ABSTRACT: The influence of docusate sodium (DOSS) on the nucleation of mefenamic acid (MEF) has been studied in different dimethylacetamide (DMA) – water mixtures. A series of induction time experiments were conducted under moderate supersaturations, varying the solvent composition and the concentration of DOSS. In 40 % DMA – 60 % water, the presence of 0.1 mg/mL and 0.2 mg/mL DOSS increased the nucleation rate. Evaluating the results by the classical nucleation theory reveals that the pre-exponential factor (A) increases by approximately 50 % while the interfacial energy is essentially uninfluenced. It is also found that the crystal growth rate becomes higher in the presence of DOSS. It is thus hypothesized that transport and desolvation of MEF molecules is facilitated in the presence of DOSS. With increasing amount of DMA in the binary solvent mixture, the influence of DOSS appears to decrease.

1. INTRODUCTION

Many potential drug candidates have poor water solubility and slow dissolution rates *in vivo*, leading to limited bioavailability and failure to reach the market¹. Antisolvent precipitation is a potential low-energy crystallization method for the industrial production of drug nanocrystals with an improved bioavailability². Additives are generally used in the process to promote nucleation, inhibit crystal growth and stabilize the system against subsequent particle transformation^{3,4}. Specifically, enhancement of nucleation can decrease the initial crystal size. By increasing the rate of nucleation, a higher number of nuclei forms and thus, smaller crystal sizes can be achieved. However, the identification of suitable additives for each drug is challenging due to the lack of knowledge about the specific action of different additives in the nanocrystal preparation process.

The mechanisms by which additives promote the nucleation of a compound is a topic of intensive interest in the crystallization community⁵. It is known that the presence of a larger amount of additive can decrease the solubility of a compound, increasing the thermodynamic driving force for nucleation. Recently, Mochizuki *et al.*⁶ found that even low concentration of additives could promote homogeneous nucleation of ice through increasing the activity of water in solution. Electrolytes were found to promote the nucleation of glycine⁷ and DL-alanine⁸ by inducing a head-to-tail molecular ordering. Computational and theoretical studies^{9,10,11,12} propose that surfactant type or surface active oligomeric additives can reduce the nucleus – solution interfacial energy and thus, reduce the nucleation work upon adsorption to the interface. In addition, additives that can stabilize the nuclei may act as heterogeneous nucleation centres^{13,14,15}.

There are only a limited number of studies showing direct experimental evidence of the promotion of nucleation of organic compounds by soluble organic additives. Kim and co-workers¹⁶ conducted induction time experiments using moderate supersaturations and found that

1
2
3 amphiphilic additives promoted the nucleation of the hexahydro-1,3,5-trinitro-1,3,5-triazine
4 molecule. However, the results showed an increasing nucleation rate over time in contrast to a
5 stationary rate assumed by the classical nucleation theory and thus, they were unable to estimate
6
7
8
9
10 interfacial energy values for the studied systems. Poornachary *et al.*¹⁷ found that
11
12 polyvinylpyrrolidone (PVP) promoted the nucleation of naproxen crystals by increasing the pre-
13
14 exponential factor with an insignificant change in the thermodynamic parameter and thus,
15
16
17 interfacial energy for nucleation. The authors concluded that PVP acted as a heterogeneous
18
19 nucleation centre in the crystallization process.
20

21
22 In an earlier study¹⁸, an anionic surfactant, docusate sodium (DOSS), had to be added to
23
24 produce nanocrystals of a poorly water-soluble compound, mefenamic acid (MEF), during an
25
26 antisolvent precipitation process in 5 % dimethylacetamide (DMA) – 95 % water system. Since
27
28 the final size of the nucleating crystals is governed by the number of formed nuclei and thus, the
29
30 nucleation rate, the reduction of the crystal size suggested that DOSS accelerated the nucleation
31
32 of MEF. The approximately threefold reduction of the crystal volume in the presence of 1 mg/mL
33
34 DOSS corresponds to a threefold increase in the number of formed nuclei, suggesting an
35
36 approximately threefold increase of the nucleation rate. An increase in nucleation rate by the
37
38 addition of additives is less commonly encountered than the opposite, so experimental evidence
39
40 that the nucleation rate actually increased is needed. In order to produce nanocrystals of MEF, a
41
42 very high supersaturation needs to be generated. This was achieved by using a high water
43
44 concentration as MEF is essentially insoluble in water. However, at these conditions the
45
46 induction time is extremely short and thus difficult to measure with sufficient accuracy. In
47
48 addition, primary nucleation is a highly stochastic process and thus the nucleation rate at each
49
50 condition must be recorded in repeated experiments. Commonly this is done in parallel cooling
51
52 crystallization experiments where 10 – 30 experiments on the millilitre scale are observed
53
54
55
56
57

1
2
3 simultaneously at isothermal conditions after the creation of supersaturation^{19,20,21} and where the
4
5 cooling and reheating can be cycled to collect perhaps a hundred recordings of the induction time
6
7 at each condition. However, supersaturation generation by cooling can only be used for induction
8
9 times in the order of minutes and longer, at lower supersaturations and water content of the
10
11 solutions, and thus not for the supersaturation experiments used in the nanocrystal manufacturing
12
13 method for mefenamic acid. Measurement of shorter induction times at higher supersaturations,
14
15 in solutions having a higher concentration of water, requires an antisolvent method. However, to
16
17 operate 50 – 100 repeated antisolvent experiments is of course much more demanding as the
18
19 antisolvent needs to be injected in every individual vial, and the experiment cannot be repeated
20
21 without replacing the solution with fresh material.
22
23
24
25

26 In this work, the influence of DOSS on the nucleation of a MEF solution is studied with the
27
28 aim being to elucidate the action of DOSS in the nanocrystal formation process of MEF. A series
29
30 of induction time experiments were performed at isothermal conditions in the absence or
31
32 presence of DOSS, varying the supersaturation and the ratio of the drug to the additive. Initially,
33
34 supersaturation was created using the conventional cooling crystallization method in 70 % DMA
35
36 – 30 % water solvent system. This allowed for parallel crystallization experiments of up to 15
37
38 vials to be performed and recycling of the solution, significantly reducing chemical waste and
39
40 labour expenses. However, no influence of DOSS on the nucleation rate was found perhaps
41
42 related to the much higher DMA content and lower supersaturations compared to the originally
43
44 used conditions during the preparation of MEF nanocrystals¹⁸. A more laborious antisolvent
45
46 crystallization method¹⁷, where the solutions had to be mixed in each separate vial to achieve a
47
48 desired composition, allowed for the study of significantly shorter induction times in 40 % DMA
49
50 – 60 % water solvent mixtures and at higher levels of supersaturation. Under these latter
51
52 conditions, DOSS enhanced the nucleation of MEF. The results are analyzed within the
53
54
55
56
57
58
59
60

framework of the classical nucleation theory (CNT), and a mechanism for the nucleation enhancement and the influence of solvent composition is proposed.

2. THEORY

According to CNT, the stationary rate of primary crystal nucleation, J , is defined as the number of crystals formed per a unit volume and time, and can be expressed as^{22,23,24}:

$$J = zf^*C^* = zf^*C_0 \exp\left(-\frac{\Delta G}{kT}\right) \quad (1)$$

where C^* is the equilibrium concentration of critical nuclei, f^* is the frequency of attachment of building units to the critical nucleus and z is the Zeldovich factor. The term C^* includes the thermodynamic information about the nucleation process, being the product of the concentration of nucleation sites in the system, C_0 , and an exponential term containing the free energy barrier, ΔG , that must be surpassed for nucleation to occur as well as the Boltzmann constant (k) and absolute temperature (T). For homogeneous nucleation assuming a spherical nucleus, ΔG can be expressed as²²:

$$\Delta G = \frac{16\pi}{3} \frac{v_m^2 \gamma^3}{(kT)^2 \ln^2 S} \quad (2)$$

where v_m is the volume of a molecule in the crystal, γ is the interfacial energy and S is the supersaturation, calculated in this paper by dividing the molar concentration (mol/L) of the molecules in the supersaturated solution with the equilibrium concentration. Note that the ratio of concentrations in the unit of mol/L for the same compound is equal to the ratio of concentrations in the unit of mg/mL, which concentration unit is also used herein for easier representation of the data.

The Zeldovich factor can be written as²²:

$$z = \frac{\ln^2 S (kT)^{3/2}}{8\pi\nu_m \gamma^{3/2}} \quad (3)$$

Attachment of monomers occurs by diffusion of the solute in the bulk solution towards the nucleus and by transferring the solute from the vicinity of the nucleus to a position incorporated in the nucleus. Assuming interface transfer control, the attachment frequency can be expressed as²²:

$$f^* = \lambda A^* c \frac{D}{d} = \lambda 8\pi \left(\frac{4\pi}{3}\right)^{1/3} \nu_m^{5/3} \gamma^2 c_{eq} D \frac{S}{(kT)^2 \ln^2 S} \quad (4)$$

where λ is the sticking coefficient accounting for the molecules in the vicinity of the nucleus that do not adsorb to the nucleus, A^* is the surface of the nucleus, c is the concentration of the monomers in the solution, d is the distance of the jump that could be approximated by the molecular diameter and D is the diffusion coefficient. D can be expressed with an Arrhenius type equation ($D=D_0\exp(-\Delta E/kT)$)²³ where ΔE describes an energy barrier associated with a desolvation process and/or conformational change of the molecule during incorporation into the nucleus. Expressing c using S and elaborating the term A^* for a spherical nuclei provides the form of the attachment frequency on the right hand side of the formula.

The above equations for the free energy barrier (2), Zeldovich factor (3), and attachment frequency (4) are derived assuming homogeneous nucleation and spherical nuclei. It is possible, however, that heterogeneous nucleation occurs on a surface that can stabilise the nucleus by lowering the interfacial energy and thus, the energy barrier for nucleation. For heterogeneous nucleation, the above formulas can be used by replacing the interfacial energy with an effective interfacial energy accounting for the influence of the heterogeneous surface²². The geometry of a non-spherical nucleus can be also considered by using numerical corrections.

By combining (1)-(4), the nucleation rate can be expressed as²²:

$$J = AS \exp\left(-\frac{B}{\ln^2 S}\right) \quad (5)$$

3. MATERIALS AND METHODS

The experimental work of this study includes determination of the solubility of mefenamic acid polymorphs (stable Form I and where relevant, metastable Form II) and nucleation induction times in 40 % DMA – 60 % water and in 70 % DMA – 30 % water, in the presence and absence of the surfactant docusate sodium. In the nucleation experiments the supersaturation is generated by antisolvent addition or cooling, respectively. For both solvent systems, the crystallized solid has been isolated for determination of the polymorphic form. In the 40 % DMA – 60 % water mixture, also the timescale of transformation of Form II to Form I has been studied.

3.1. Materials

Mefenamic acid (MEF, Form I, >98 %), *N,N*-dimethylacetamide (DMA, >99.9 %), acetonitrile (ACN), acetic acid, sodium docusate (dioctyl sulfosuccinate sodium salt, DOSS), and sodium acetate were obtained from Sigma Aldrich. Tetrahydrofuran (THF) was purchased from VWR. Deionized water was used for aqueous solutions (18 M Ω , ELGA, Purelab Ultra). All chemicals were used as received.

The metastable polymorphic form, MEF Form II, was prepared as a reference material by heating the as received MEF Form I to 160 °C for 48 hours²⁵. The structural purity of the product was examined by PXRD and FTIR.

3.2. Solubility Studies

The solubility of the stable MEF polymorph, Form I in 40 % DMA – 60 % water (v/v) was determined at the crystallization temperature (T_{cryst}) of 25 °C in the absence and presence of 0.2

1
2
3 mg/mL DOSS from six separate solubility experiments. Here v/v % represents the volume
4
5 fraction of solvents mixed for creating the specific cosolvent system. The solubility of Form I in
6
7 70 % DMA – 30 % water (v/v) was measured at the crystallization temperature (T_{cryst}) of 15 °C
8
9 in the presence of 0-5 mg/mL DOSS, as well as at 20 °C, 30 °C and 35 °C in the absence of
10
11 DOSS to estimate the saturation temperature (T_{sat}) at which a solution with a given concentration
12
13 is saturated. In this solvent system, three separate solubility experiments were done at each
14
15 condition of DOSS concentration and temperature. In all cases, solutions were saturated by
16
17 adding an excess of Form I solid to the corresponding solvent mixture and placing into a water
18
19 bath (Grant GR150, accuracy ± 0.1 °C) under magnetic stirring at 400 rpm. After 24 h, the stirrer
20
21 was switched off and the suspensions were left to settle for 24 h. From each solution a 2 mL
22
23 sample was then filtered with nylon (with 40 % DMA) or polytetrafluoroethylene (PTFE) (with
24
25 70 % DMA) syringe filters (0.2 μm pore size, VWR), discarding the first mL to avoid possible
26
27 adsorption of the MEF molecules to the filter membrane. While a hydrophilic nylon membrane
28
29 was suitable for filtering solutions containing 60 % water, an organic solvent resistant PTFE was
30
31 used to avoid possible degradation of the filter material with 70 % DMA. In case of both solvent
32
33 systems, the filtrate was diluted with 70 % DMA – 30 % water and analyzed using an Agilent
34
35 high performance liquid chromatography system (HPLC) at a detection wavelength of 285 nm.
36
37 The mobile phase consisted of 55 % sodium acetate buffer at 50 mM, pH 5 and 45 % ACN:THF
38
39 (23:7) solvent mixture. The chromatographic separation was carried out using a reverse phase C_8
40
41 column (250 mm x 4.6 mm) and 1 mL/min flow rate. The volume of the injected sample was 20
42
43 μL . Powder X-ray diffraction experiments verified that the crystalline state of the suspended
44
45 MEF Form I did not change during the equilibration.
46
47
48
49
50
51
52

53 The determination of the solubility of the metastable Form II polymorph is more challenging
54
55 because of the tendency for polymorphic transformation. Thus in the present work, the solubility
56
57

1
2
3 of Form II crystals was estimated from the mole fraction solubility ratio (x^{II}/x^I) determined by
4
5 Romero *et al.*²⁶ at 25.0 °C in different solvents, as this value is almost independent of the choice
6
7 of solvent, representing the relative stability of the forms at a certain temperature (fundamental
8
9 justification is given in Supporting Information). The mole fraction solubility ratio of MEF Form
10
11 II and Form I at 25.0 °C was reported to be 1.37 in water, 1.40 in ethanol and 1.28 in ethyl
12
13 acetate²⁶. Considering that polymorphic transformation is the fastest when the solubility is the
14
15 highest, *i.e.* in ethyl acetate²⁶, and the solubility determination is more uncertain at low solubility,
16
17 *i.e.* in water²⁶, the highest mole fraction solubility ratio measured in ethanol, 1.40, has been
18
19 selected for the solubility calculation of MEF Form II at 25.0 °C.
20
21
22

23
24 In 40 % DMA – 60 % water at 25.0 °C, the solubility of the stable MEF Form I was $0.065 \pm$
25
26 0.003 mg/mL, and remained the same in the presence of 0.2 mg/mL DOSS (Table 1). The
27
28 solubility of the metastable MEF Form II was calculated to be 0.091 ± 0.004 mg/mL. In 70 %
29
30 DMA – 30 % water the solubility of MEF Form I at 15.0 °C was 3.80 ± 0.01 mg/mL and did not
31
32 change in the presence of 1 mg/mL DOSS but increased slightly to 3.92 ± 0.03 mg/mL in the
33
34 presence of 5 mg/mL DOSS. The solubility in 70 % DMA – 30 % water in the absence of DOSS
35
36 determined at different temperatures are graphed on Figure S1 (Supporting Information) along
37
38 with an exponential fit to calculate Form I saturation temperatures for any given concentration
39
40 relevant to supersaturation generation by cooling crystallization.
41
42
43
44
45
46
47

48 Table 1 Solubility of MEF in 40 % DMA – 60 % water at 25 °C and in 70 % DMA – 30 % water
49
50 at 15 °C in the absence and presence of different concentrations of DOSS. Standard deviation is
51
52 calculated from six (40 % DMA – 60 % w) or three (70 % DMA – 30 % w) repeat of the entire
53
54 solubility determination experiment.
55
56
57

DOSS / mg·mL ⁻¹	Solubility in 40 % DMA – 60 % w at 25 °C / mg·mL ⁻¹		Solubility in 70 % DMA – 30 % w at 15 °C / mg·mL ⁻¹
	Form I	Form II	Form I
0	0.065 ± 0.003	0.091 ± 0.004*	3.80 ± 0.01
0.1	-	-	3.81 ± 0.01
0.2	0.065 ± 0.001	0.091 ± 0.002*	-
1	-	-	3.81 ± 0.03
2.5	-	-	3.84 ± 0.04
5	-	-	3.92 ± 0.03

* calculated from Form I solubility using the mole fraction solubility ratio of $x^{\text{II}}/x^{\text{I}}=1.4$

3.3. Induction time experiments

Induction time refers to the time elapsed from the moment of the creation of supersaturation until the detection of the first crystals. Two different procedures, antisolvent crystallization (40 % DMA – 60 % water) and cooling crystallization, were used to generate supersaturation. Although supersaturation generation was different, crystallization occurred at isothermal conditions in both crystallization procedures at relatively similar temperatures, providing a basis for the comparison of the results. The program of induction time experiments is presented in Table 2, including the temperature of crystallization, the polymorphic outcome and supersaturations calculated based on the solubility results from Table 1. Throughout the paper, S^{I} denotes supersaturation calculated with respect to Form I, whereas S^{II} denotes supersaturation calculated with respect to Form II. Polymorphic behavior of the systems, providing a basis for the calculation of supersaturation, is presented later, in section 4.1. In both systems, the concentration of DOSS was selected to achieve molar ratios comparable to the originally used $n_{\text{DOSS}}/n_{\text{MEF}}=0.29$ during the preparation of MEF nanocrystals in 5 % DMA – 95 % water¹⁸.

Table 2. Induction time experiments performed, temperature of crystallization (T_{cryst}), concentration of MEF (c_{MEF}) and DOSS (c_{DOSS}) in the final solvent mixture, the molar ratio of DOSS to MEF ($n_{\text{DOSS}}/n_{\text{MEF}}$), nucleating polymorphic form and supersaturation (S)

% (v/v) of DMA	Generation of supersaturation	$T_{\text{cryst}} / ^\circ\text{C}$	$c_{\text{MEF}} / \text{mg}\cdot\text{mL}^{-1}$	$c_{\text{DOSS}} / \text{mg}\cdot\text{mL}^{-1}$	$n_{\text{DOSS}}/n_{\text{MEF}}$	Polymorphic form	S
40	Antisolvent crystallization	25	0.40	0	0	Form II	4.40 ^{II}
				0.1	0.14		
				0.2	0.27		
			0.30	0	0	Form II	3.30 ^{II}
				0.1	0.18		
				0.2	0.36		
			0.24	0	0	Form II	2.64 ^{II}
				0.1	0.23		
				0.2	0.45		
			0.20	0	0	Form II	2.20 ^{II}
				0.1	0.27		
				0.2	0.54		
70	Cooling crystallization	15	7.55	0	0	Form I	1.99 ^I
			6.66	0	0	Form I	1.75 ^I
				1	0.08		1.70 ^I
			5	0.41			
5.81	0	0	Form I	1.53 ^I			

^IS is calculated based on Form I solubility

^{II}S is calculated based on Form II solubility

In the case of the 40 % DMA – 60 % water solvent system, supersaturation ($S^{\text{II}}=4.40 - 2.20$) was created by antisolvent crystallization at $T_{\text{cryst}}=25.0$ °C. MEF solution (solution 1) was prepared in 80 % DMA – 20 % water (v/v) and filtered with a PTFE syringe filter (0.2 μm , VWR) after overnight stirring. The antisolvent solution (solution 2) consisted of 5.9 mL deionised water or aqueous DOSS solution premixed with 3.6 mL DMA. When DOSS was used,

1
2
3 the antisolvent solution was filtered with a nylon syringe filter (0.2 μm , VWR) to remove
4
5 particulate impurities. For an induction time experiment, 0.5 mL MEF solution (solution 1) was
6
7 pipetted into 9.5 mL antisolvent solution (solution 2) giving a final solvent composition of 40 %
8
9 DMA – 60 % water. The mixed solution was stirred at 300 rpm using a magnetic stir bar and the
10
11 induction time was recorded with a camera. The visually detectable level of the mixing of the two
12
13 phases was complete within 4 s. Since the mixing of DMA and water is highly exothermic,
14
15 premixing of the major part of DMA and water as the antisolvent solution prior the addition of
16
17 MEF solution allowed for the reduction of the initial temperature rise to less than 0.2 $^{\circ}\text{C}$. The
18
19 recorded videos were analyzed by the naked eye, carefully comparing snapshots prior to and after
20
21 the visual appearance of crystals. The uncertainty of the detection technique itself, estimated from
22
23 repeated analysis of the induction time video for a given vial of nucleating solution is 3-4 seconds
24
25 at $S^{\text{II}}=4.40$, increasing to 5-10 s at $S^{\text{II}}=2.20$. The use of lower supersaturations was restricted due
26
27 to the decreasing turbidity of the system as a result of the lower mass crystallized. A 59-91 data
28
29 points were measured for each condition to account for the stochastic nature of nucleation.
30
31
32
33
34

35 In the case of 70 % DMA – 30 % water, supersaturation ($S^{\text{I}}=1.99 - 1.53$) was generated by
36
37 cooling the solution below its saturation temperature, to $T_{\text{cryst}}=15^{\circ}\text{C}$. A 250 mL stock solution
38
39 was prepared by dissolving a known amount of MEF in the premixed solvent mixture at a T_{diss}
40
41 dissolution temperature, 16 $^{\circ}\text{C}$ above the corresponding saturation temperature ($T_{\text{diss}}=T_{\text{sat}}+16^{\circ}\text{C}$)
42
43 using submersible magnetic stirrer plate for mixing (400 rpm, 4 h). Based on solubility results
44
45 (Figure S1 in Supporting Information), T_{diss} was 40.0 $^{\circ}\text{C}$, 42.8 $^{\circ}\text{C}$ and 45.0 $^{\circ}\text{C}$ for $S^{\text{I}}= 1.53$,
46
47 $S^{\text{I}}=1.75$ and $S^{\text{I}}=1.99$, respectively. Then, the solution was filtered with preheated syringes
48
49 equipped with PTFE filters (0.2 μm , VWR) to eliminate particulate impurities. This batch
50
51 solution was subjected to two crystallization cycles prior to recording any induction times (pre-
52
53 treatment cycles) in order to overcome history of solution/filtration effects: first crystallization at
54
55
56
57
58
59
60

1
2
3 5 °C followed by dissolution of the crystals at T_{diss} (4 h), then crystallization at $T_{\text{cryst}}=15$ °C
4 followed by dissolution of the crystals at T_{diss} (3 h). Fifteen mL solutions were then distributed
5
6 into 15 preheated vials containing a magnetic stir bar and left to equilibrate for another 2 h at
7
8 T_{diss} . To start the induction time experiments, the vials were placed into a waterbath at
9
10 $T_{\text{cryst}}=15$ °C and stirrer speed of 250 rpm, and a high resolution camera was started to record the
11
12 induction time by visual inspection. Due to the 3-4 min initial cooling period to the crystallization
13
14 temperature, also measured as a part of the induction time, only supersaturations giving
15
16 sufficiently large induction times (>10 min) could be studied using this method to ensure that
17
18 nucleation occurs at isothermal conditions. After crystallization, the vials were placed back into
19
20 the waterbath at T_{diss} for dissolution (5 h) and the crystallization cycle was repeated ($T_{\text{cryst}} - T_{\text{diss}} -$
21
22 T_{cryst} and so on) to collect 90-105 and 60-75 induction time data in the absence and presence of
23
24 DOSS, respectively.
25
26
27
28
29

30 31 **3.4. Isolation and characterization of the crystals**

32
33 In the case of 40 % DMA – 60 % water solvent system, two drying methods have been used to
34 understand the polymorphic behavior of the systems. (1) At $S^{\text{II}}=4.40$ in the absence of DOSS,
35 crystals were isolated by filtration at different times (8 min, 15 min and 3.5 hours) after the first
36
37 detection of crystallization and dried under high vacuum (<27 Pa) at room temperature for 16 h.
38
39 (2) At $S^{\text{II}}=4.40$ and $S^{\text{II}}=2.20$, in the absence and presence of 0.1-0.2 mg/mL DOSS, crystals were
40
41 isolated by filtration, 8 min (in case of $S^{\text{II}}=4.40$) or 15 min (in case of $S^{\text{II}}=2.20$) after the first
42
43 detection of crystallization and dried at 50 °C for 1 h. Due to the very low crystallizing mass,
44
45 these selected times were required to ensure enough sample for characterization. While drying at
46
47 room temperature was employed to slow down polymorphic transformation during drying, the
48
49 obtained crystals were partially defected because of the high vacuum. Thus, the second drying
50
51
52
53
54
55
56
57
58
59
60

1
2
3 method using higher temperature but atmospheric pressure was used further on to avoid
4
5 sublimation of the crystals.
6

7
8 In case of 70% DMA – 30 % water, crystals were isolated by filtration, 8 min ($S^I=1.99$) or 15-
9
10 20 min ($S^I=1.75$ and $S^I=1.70$) after the first detection of crystallization and dried at 50 °C for 1
11
12 hour.
13

14
15 The polymorphic form of the crystals, in cases of small crystallization yields, was
16
17 characterized by Fourier transform infrared (IR) spectroscopy, employing a Perkin Elmer
18
19 Spectrum 100 ATR FTIR. Spectra were recorded between 650-4000 cm^{-1} using 2 cm^{-1} spectral
20
21 resolution and 32 scan per sample. Three samples were characterized at each condition unless
22
23 otherwise stated.
24
25

26
27 The polymorphic form of the crystals nucleated in 70 % DMA – 30 % water at $S^I=1.99$,
28
29 having a larger crystallization yield, was verified using a Philips PANalytical X'pert powder X-
30
31 ray diffractometer. The sample was placed between amorphous tapes and measured in
32
33 transmission geometry using Ni filtered Cu $K\alpha$ radiation ($\lambda=1.54 \text{ \AA}$), 40 kV accelerating voltage
34
35 and 40 mA anode current. The diffraction pattern was collected between 5° and 30° (2θ) and the
36
37 separately measured diffraction pattern of the amorphous tape was subtracted from the
38
39 diffractogram.
40
41

42
43 The size and habit of the isolated crystals were analyzed by a HITACHI SU-70 scanning
44
45 electron microscope at 3 kV. To prepare the samples, a small amount of isolated particle was
46
47 placed onto an adhesive carbon tape attached to a cylindrical aluminum sample holder and gold
48
49 sputtered at 20 mA for 1 minute using an EMITECH K550. Two samples were characterized at
50
51 each condition.
52
53
54
55
56
57
58
59
60

4. RESULTS

4.1. Polymorphic behaviour of the systems

Example IR spectra of the crystals nucleated in 40 % DMA – 60 % water at $S^{II}=4.40$ and $S^{II}=2.20$ in the absence and presence of 0.1-0.2 mg/mL DOSS and dried at 50 °C are shown in Figure 1, whereas additional spectra of repeated samples are shown in Figure S2 ($S^{II}=4.40$) and in Figure S3 ($S^{II}=2.20$) in the Supporting Information. The stable Form I and the metastable Form II polymorphs can be distinguished by the band position associated with the amine stretch^{25,27}, being 3308 cm⁻¹ with a shoulder at 3344 cm⁻¹ for Form I and a single peak at 3344 cm⁻¹ for Form II. Looking at $S^{II}=4.40$ in Figure 1 and Figure S2, several samples contain only Form II crystals and in case of the mixtures, Form II crystals are dominating with a small amount of Form I. This indicates that the metastable Form II crystals are nucleating initially and the stable Form I crystals appear as a result of polymorphic transformation. At $S^{II}=2.20$ shown in Figure 1 and Figure S3, the majority of the isolated samples are a mixture of Form II and Form I crystals (eight out of nine samples) with one exception at 0.2 mg/mL DOSS being only Form I. The higher ratio of Form I crystals in these samples as opposed to at $S^{II}=4.40$ is likely to be the result of longer suspension aging time, being 15 min as opposed to 8 min at $S^{II}=4.40$. At both supersaturations, no clear influence of DOSS on the polymorphic form was observed.

The timescale of polymorphic transformation was tested at $S^{II}=4.40$ in the absence of DOSS by isolating samples at different times after the detection of crystallization and drying under high vacuum at room temperature. Compared to drying at 50 °C (Figure 1), this drying condition provided pure Form II samples or samples containing a significantly lower amount of Form I crystals when isolated after the same 8 min aging time (Figure S4 in Supporting Information). Increasing the aging time to 15 min substantially increased the amount of Form I crystals in the sample, and after 3.5 h aging pure Form I crystals or Form I crystals with a very small amount of

Form II were obtained. These results verify that the timescale of polymorphic transformation is indeed short and even more accelerated by drying at higher temperatures, supporting the hypothesis that the presence of Form I crystals in the samples crystallized at $S^{\text{II}}=4.40$ or $S^{\text{II}}=2.20$ and dried at 50 °C is due to polymorphic transformation. Therefore supersaturation is calculated with respect to Form II solubility in 40 % DMA – 60 % water systems.

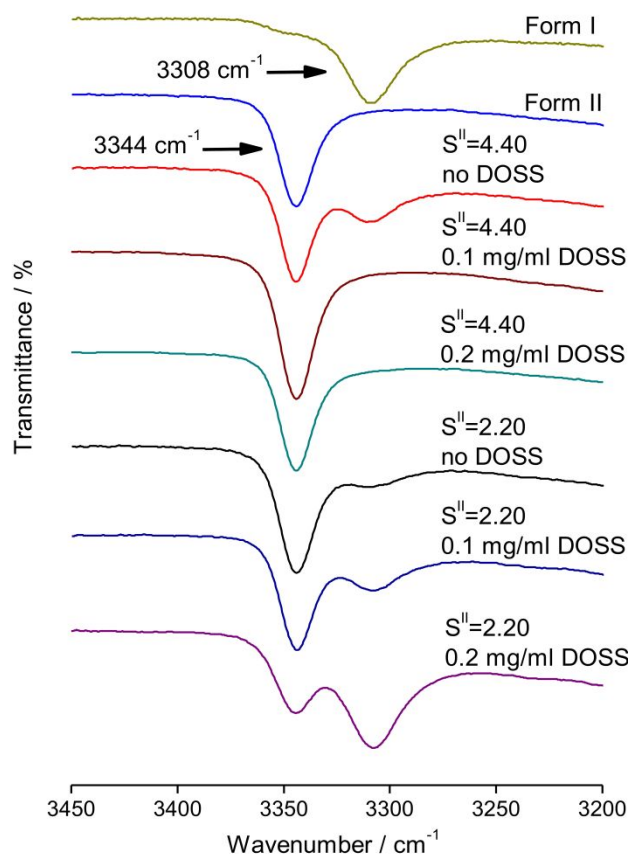


Figure 1 IR spectra of pure MEF polymorphs and MEF crystals nucleated in the absence or presence of DOSS at different supersaturations. At $S^{\text{II}}=4.40$, crystals were isolated at 8 min aging time, whereas at $S^{\text{II}}=2.20$, crystals were isolated after 15 min aging time, and crystals were dried at 50 °C. S^{II} is calculated based on the solubility of the nucleating Form II crystals.

In 70 % DMA – 30 % water, in the pure MEF system at $S^{\text{I}}=1.99$, Form I crystals were isolated (Figure 2). Since Form I crystals have a weak adsorption band in the IR spectra at the same

position as the main band of Form II crystals, 3344 cm^{-1} , the absence of Form II crystals in the sample was verified using PXRD (Figure S5 in Supporting Information). At $S^I=1.75$, the addition of 1 mg/mL and 5 mg/mL DOSS did not have an influence on the polymorphic form of the crystals, yielding Form I crystals in each case. Since only the stable polymorphic form was isolated at $S^I=1.99$ and $S^I=1.75$, the crystals at $S^I=1.53$ are also expected to be Form I. Therefore supersaturation is calculated with respect to Form I solubility in 70% DMA – 30% water systems.

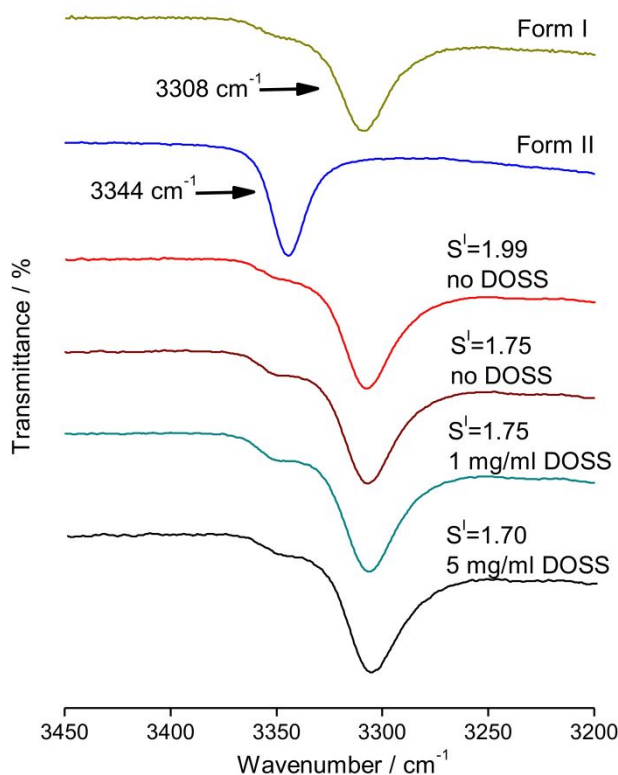


Figure 2 IR spectra of pure MEF polymorphs and MEF crystals nucleated in the absence or presence of DOSS at different supersaturations. At $S^I=1.99$, crystals were isolated at 8 min aging time, whereas at $S^I=1.75$ and 1.70 , crystals were isolated after 15-20 min aging time. S^I is calculated based on the solubility of the nucleating Form I crystals.

Figure 3 presents SEM images of the crystals obtained from 40 % DMA – 60 % water. Based on IR, most of the samples presented herein are a mixture of Form I and Form II crystals (except at $S^{II}=4.40$, 0.1 mg/mL DOSS) with the images focusing on the initially nucleating Form II crystals. In the absence of DOSS, Form II crystals had parallelepiped habit at both $S^{II}=4.40$ and $S^{II}=2.20$, having more evolved facets at $S^{II}=2.20$. The presence of DOSS, irrespective of the concentration used, did not have a noticeable influence on the habit indicating no specific face for adsorption of the surfactant molecule. The habit of Form I crystals present in the same samples, when found in the case of polymorph mixtures, was distinctly different being plate-like at all studied conditions (Figure S6 in Supporting Information). Similarly, in 70 % DMA – 30 % water at $S^I=1.75$ in the absence of DOSS, the habit of the Form I crystals was plate-like, and did not change upon the addition of 1 mg/mL or 5 mg/mL DOSS (Figure 4.)

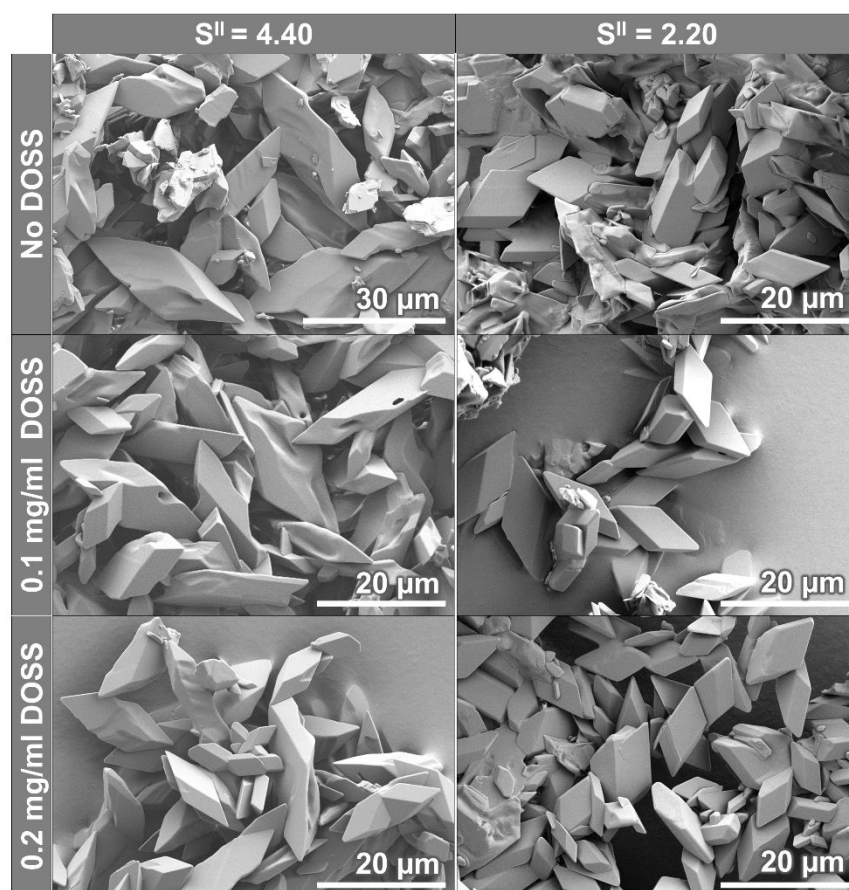


Figure 3 SEM images of MEF crystals prepared in the absence or presence of DOSS in 40 % DMA – 60 % water, at $S^{\text{II}}=4.40$ (isolated at 8 min) and at $S^{\text{II}}=2.20$ (isolated at 15 min). Based on IR, samples are a mixture of Form I and Form II crystals except at $S^{\text{II}}=4.40$, 0.1 mg/mL DOSS, with the images focusing on mainly Form II crystals (parallelepiped shape). S^{II} is calculated based on Form I solubility.



Figure 4 SEM images of crystals prepared in the absence and presence of DOSS in 70 % DMA – 30 % water. Crystals were isolated after 15-20 min aging and are pure Form I. S^{I} is calculated based on Form I solubility.

4.2. Induction time probability distributions

Figure 5 shows the experimental probability distribution of induction times of MEF in 40 % DMA – 60 % water at $S^{\text{II}}=4.40-2.20$ in the absence or presence of 0.1 mg/mL and 0.2 mg/mL DOSS. For each system, the induction times and the width of the distributions are systematically increasing with decreasing supersaturation, where the scattering of the data is attributed to the inherent stochasticity of nucleation events^{28,29,30} and influenced by the experimental technique used³¹. In the absence of DOSS, the measured induction times were in the range of 27 s – 74 s at $S^{\text{II}}=4.40$ and increased to 92 s – 370 s with decreasing the supersaturation to $S^{\text{II}}=2.20$. In the presence of DOSS, overall shorter induction times were measured at each supersaturation examined but the measured distributions did not depend on the DOSS concentration.

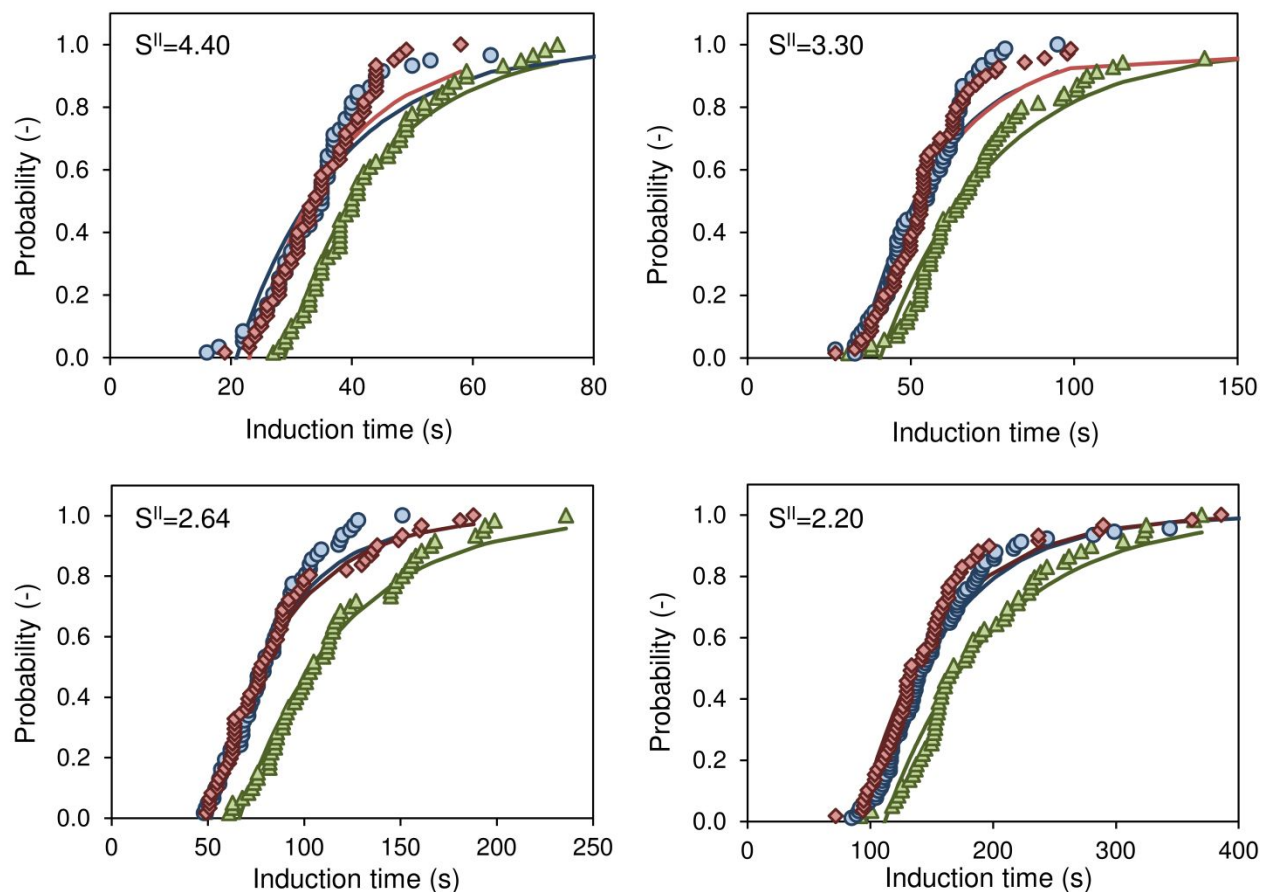


Figure 5 Experimental probability distributions of induction times of MEF in the absence or presence of DOSS at different supersaturations. Green triangle (Δ): pure MEF; blue circle (\circ): MEF with 0.1 mg/mL DOSS; red rhombus (\diamond): MEF with 0.2 mg/mL DOSS. The fit to equation (6), described in section 4.3, is also shown. S^{II} is calculated based on the solubility of the nucleating Form II crystals.

In a 70 % DMA – 30 % water solvent mixture, presented in Figure 6, the induction times varied from ten minutes to hours at $S^I=1.99$ -1.53, in contrast to induction times of couple of ten seconds to minutes measured in 40 % DMA – 60 % water systems at higher supersaturations. At $S^I=1.75$, the addition of 1 mg/mL DOSS only slightly shifted the distribution to longer induction times compared to the pure system. In the presence of 5 mg/mL, the supersaturation decreased

from $S^I=1.75$ to $S^I=1.70$ at the same concentration of MEF due to the increase in solubility. The corresponding induction time distribution was shifted to longer induction times compared to the two systems at $S^I=1.75$.

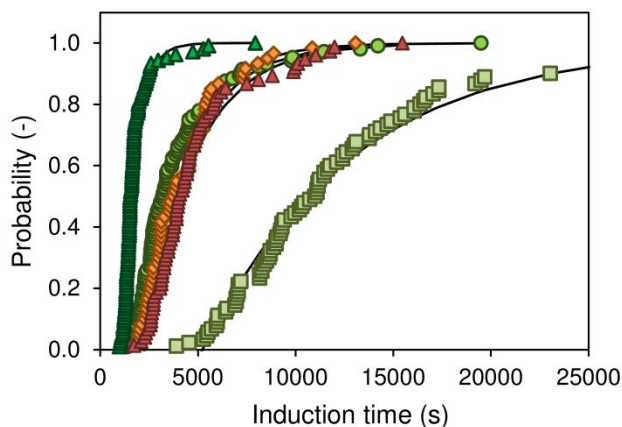


Figure 6 Experimental probability distributions of induction times of MEF in the absence or presence of DOSS at different supersaturations in 70 % DMA – 30 % water. Dark green triangle (▲): pure MEF at $S^I=1.99$; green circle (●): pure MEF at $S^I=1.75$; light green square (■): pure MEF at $S^I=1.53$; orange rhombus (◆): MEF with 1 mg/mL DOSS at $S^I=1.75$; red triangle (▲): MEF with 5 mg/mL DOSS at $S^I=1.70$. Fit to equation (6), described in section 4.3, is also shown. S^I is calculated based on the solubility of the nucleating Form I crystals.

4.3. Nucleation rate determination

Assuming independent nucleation events and a single nucleus mechanism, the induction time distributions can be described with a homogeneous Poisson distribution, where the probability of detection of a nucleation event $P(t)$ within a time t is^{21,24,32}:

$$P(t) = 1 - \exp(-J \cdot V(t - t_g)) \quad (6)$$

Where J is the nucleation rate, V is the solution volume and t_g is the growth time. The growth time accounts for the time difference between the detection of nucleation (t) and the actual nucleation event ($t-t_g$), with the assumption that the shortest nucleation time is 0 s ($t=t_g$). Tables 3 and 4 summarize J and t_g obtained from fitting equation (6) to the experimental probability distributions presented in Figure 5 and 6, respectively. In 40 % DMA – 60 % water, R^2 values describing the quality of the fit were in the range of 0.89-0.99, being lower at higher supersaturations, whereas in 70 % DMA – 30 % water, a fairly good $R^2 \geq 0.95$ was found at all conditions.

In 40 % DMA – 60 % water (Table 3), in the presence of DOSS, the nucleation rate increased by 37-51 %, while the growth time decreased by 13-22 % compared to the pure system in the range of $S^{II}=2.20-3.30$, with no major difference between the studied DOSS concentrations. At $S^{II}=4.40$, the experimental induction time distributions from Figure 5 shows the same trend. However, the analysis, Table 3, lead to significantly lower nucleation rate at $S^{II}=4.40$ in the presence of 0.1 mg/mL DOSS than in the presence of 0.2 mg/mL DOSS or in the absence of DOSS. These outlying data points arise from the increasing uncertainty of the results with increasing supersaturation and the lowest accuracy of the Poisson fit at $S^{II}=4.40$ in the presence of 0.1 mg/mL DOSS ($R^2=0.89$).

As a comparison, to verify the same influence of DOSS at $S^{II}=4.40$ as at $S^{II}=3.30-2.20$, we also determined J from fitting a lognormal cumulative distribution function (LCDF)^{20,33}:

$$P(t) = 0.5 \operatorname{erfc}(-(\ln t - \eta) / \sigma \sqrt{2}) \quad (7)$$

to the cumulative induction time distributions, where the location parameter η can be translated to the geometric mean (=median induction time, t_{50}) by $\exp(\eta) = t_{50}$ and the scale parameter σ to the geometric standard deviation (σ^*) by $\exp(\sigma) = \sigma^*$. The nucleation rate, included in Table 3, can be

1
2
3 calculated from the median induction time and solution volume by $J = 1/t_{50}V$. Compared to J
4
5 values obtained using the Poisson function (6), using LCDF resulted in a similar trend in the
6
7 range of $S^{II}=2.20-3.30$, with values being 47-55 % smaller. This trend also extended to $S^{II}=4.40$,
8
9 showing higher and comparable nucleation rates in the presence of both concentration of DOSS
10
11 than in the absence of it. The difference in the nucleation rates calculated by fitting a Poisson
12
13 distribution and the LCDF derives primarily from the fact that the latter method assumes that the
14
15 time to grow to visibility is negligible. Thus, the nucleation time is approximated by the
16
17 induction time, and the nucleation rate is calculated from the median induction time. This results
18
19 in larger nucleation times and thus, lower nucleation rates. However, in these systems, it appears
20
21 as if the growth time is not negligible and thus, the LCDF analysis is primarily presented to
22
23 qualitatively verify the trend in nucleation rates at different supersaturations and DOSS
24
25 concentrations, as this analysis is less sensitive to the shape of induction time distribution than
26
27 the Poisson analysis.
28
29
30
31
32
33
34
35
36
37
38
39
40
41
42
43
44
45
46
47
48
49
50
51
52
53
54
55
56
57
58
59
60

Table 3. Nucleation rate, J , and growth time, t_g , of MEF at different S^{II} supersaturations in the absence or presence of DOSS in 40 % DMA – 60 % water, from fitting to equation (6). As a comparison, the median induction time t_{50}^a and the nucleation rate J^a from fitting to equation (7) is also shown. S^{II} is calculated based on the solubility of the nucleating Form II crystals.

S^{II}	DOSS / mg·mL ⁻¹	Molar ratio $n_{\text{DOSS}}/n_{\text{MEF}}$	J /m ⁻³ s ⁻¹	t_g /s	t_{50}^a /s	J^a /m ⁻³ s ⁻¹
4.40	0.0	0	6270	28.8	40.9	2448
4.40	0.1	0.14	5784	20.8	33.5	2982
4.40	0.2	0.27	7025	23.0	33.8	2956
3.30	0.0	0	2861	40.6	65.6	1524
3.30	0.1	0.18	4061	33.9	52.6	1901
3.30	0.2	0.36	4027	34.7	52.9	1890
2.64	0.0	0	1859	66.3	106.2	941
2.64	0.1	0.23	2799	51.6	78.8	1267
2.64	0.2	0.45	2606	50.7	78.9	1267
2.20	0.0	0	1109	111.4	177.1	565
2.20	0.1	0.27	1517	96.8	145.2	689
2.20	0.2	0.54	1524	90.5	141.3	723

In 70 % DMA – 30 % water at $S^{\text{I}}=1.99-1.53$ (Table 4), the nucleation rates determined by fitting the Poisson function were orders of magnitude lower and the growth times larger compared to those measured at higher supersaturations in 40 % DMA – 60 % water. At $S^{\text{I}}=1.75$, compared to the pure system, the addition of 1 mg/mL DOSS only slightly decreased the nucleation rate by 7 %, but increased the growth time by 20 %. At $S^{\text{I}}=1.70$ in the presence of 5 mg/mL DOSS, the nucleation rate was further decreased and the growth time increased, possibly just because of the lower supersaturation.

Table 4. Nucleation rate, J , and growth time, t_g , of MEF at different S^I supersaturations in the absence or presence of DOSS in 70 % DMA – 30 % water, from fitting to equation (6). S^I is calculated based on Form I solubility.

S^I	DOSS / mg·mL ⁻¹	Molar ratio $n_{\text{DOSS}}/n_{\text{MEF}}$	J /m ⁻³ s ⁻¹	t_g /s
1.99	0	0	104.2	1128
1.75	0	0	28.9	1638
1.75	1	0.08	26.8	1972
1.70	5	0.41	25.7	2259
1.53	0	0	8.6	5239

4.4. Calculation of pre-exponential factor and interfacial energy

In order to calculate the pre-exponential factor A and interfacial energy γ of the nucleation process, equation (5) can be rearranged using $B'=B \cdot T^3$ as:

$$\ln \frac{J}{S} = \ln A - \frac{B'}{T^3 \ln^2 S} \quad (8)$$

This shows that a plot of $\ln (J/S)$ versus $T^{-3} \ln^{-2} S$ should result in a straight line with an intercept of $\ln A$ and a slope of $-B'$. From B' , the interfacial energy, γ , can be calculated as:

$$B' = \frac{16\pi}{3} \frac{\gamma^3 v_m^2}{k^3} \quad (9)$$

Figure 7a and Figure S7 in Supporting Information show this fit for the nucleation rates measured in 40 % DMA – 60 % water excluding and including $S^{II}=4.40$ in the linear fit, respectively, whereas Figure 7b presents the plot in both solvent systems and shows the fit for pure MEF in 70 % DMA – 30 % water. The nucleation parameters calculated from the fits are summarized in Table 5.

1
2
3 In 40 % DMA – 60 % water, the nucleation parameters were calculated excluding and
4 including the outlying $S^{II}=4.40$ in the linear regression. Excluding $S^{II}=4.40$ from the linear
5 regression provided an excellent linear correlation for all the three systems ($0.98 \leq R^2$). From the
6 fits, the pre-exponential factor A was calculated to be $1324 \text{ m}^{-3}\text{s}^{-1}$ in the absence of DOSS and
7 increased to $2007 \text{ m}^{-3}\text{s}^{-1}$ and $1904 \text{ m}^{-3}\text{s}^{-1}$ with the addition of 0.1 mg/mL and 0.2 mg/mL DOSS,
8 respectively. In contrast, the interfacial energy γ (with respect to Form II) was similar in the
9 absence or presence of DOSS, being $2.92 - 3.00 \text{ mJm}^{-2}$. Including $S^{II}=4.40$, the fit was less good
10 ($0.91 \leq R^2$) and the derived A and γ values did not show a clear trend with changing the
11 concentration of DOSS from 0 to 0.2 mg/mL . Thus nucleation parameters at $40 \text{ \% DMA} - 60 \text{ \%}$
12 water are determined using the Poisson fit, excluding the data points at $S^{II}=4.40$, which may
13 deviate because uniformity of supersaturation might not have been achieved at the shortest
14 induction times. The mixing of the solvent and antisolvent solutions is visually detectable for
15 approximately 4 s after solution injection, and molecular level mixing should be somewhat longer
16 than this. As a comparison, at the highest supersaturation of $S^{II}=4.40$, the shortest induction time
17 data is 16 s , whereas at the second highest supersaturation of $S^{II}=3.30$ this data is 27 s , being
18 considerable longer.

19
20
21
22
23
24
25
26
27
28
29
30
31
32
33
34
35
36
37
38
39
40 As an estimation for the error of calculating the solubility of Form II and the corresponding
41 S^{II} from the mole fraction solubility ratio of $x^{II}/x^I=1.4$, A and γ values have been recalculated
42 using $x^{II}/x^I=1.3$ or $x^{II}/x^I=1.5$. The obtained results are qualitatively the same, with A and γ values
43 being $2.0-2.3 \text{ \%}$ smaller and 7.9 \% larger at $x^{II}/x^I=1.3$, respectively, and $1.9-2.2 \text{ \%}$ larger and 7.4
44
45
46
47
48
49
50
51
52
53
54
55
56
57
58
59
60
% smaller at $x^{II}/x^I=1.5$, respectively, and showing no influence of DOSS on γ .

As can be seen from Table 5, the same trend in A^a and similar γ^a values were found when the
parameters were calculated from plotting the nucleation rates determined from fitting to LCDF
(J^a) in the whole range of studied supersaturations, $S^{II}=2.20-4.40$, as for A and γ over $S^{II}=2.20-$

1
2
3 3.30. This verifies that DOSS only has an effect on the pre-exponential factor with an
4 insignificant influence on the interfacial energy.
5
6

7
8 In previous recent work on tolbutamide³⁴ survival theory analysis has been adopted for
9 advanced evaluation of the statistical confidence of parameters obtained by fitting the classical
10 nucleation theory to the same kind of nucleation data as in this study. In the study of tolbutamide
11 in different solvents slopes and intercepts depending on the solvent were proven to be statistically
12 different, except for between the two alcohols that also in the graph essentially overlapped. In the
13 tolbutamide study 50-100 induction times were determined for each of three different
14 supersaturations except for one case where there were four different supersaturations. In the
15 present study on mefenamic acid 59-91 induction times were determined for each of three
16 different supersaturations ($S^{\text{II}}=3.30-2.20$) in 40 % DMA - 60 % water. Accordingly the statistical
17 conditions are very similar, and based on this experience and the appearance of the classical
18 nucleation theory plot (Figure 7a) we believe that it is reasonable to assume that there is a
19 statistically valid difference in the nucleation behavior between the pure solution and the impure
20 solutions.
21
22
23
24
25
26
27
28
29
30
31
32
33
34
35
36

37 In 70 % DMA – 30% water, in the absence of DOSS, the pre-exponential factor was found to
38 be $A=160 \text{ m}^{-3}\text{s}^{-1}$ and the interfacial energy was calculated to be $\gamma = 2.86 \text{ mJm}^{-2}$ with respect to
39 Form I. The data points with 1 mg/mL DOSS at $S^{\text{I}}=1.75$ and 5 mg/mL DOSS at $S^{\text{I}}=1.70$ are lying
40 along the fitted line of the pure system within experimental error, suggesting no influence on the
41 nucleation of MEF.
42
43
44
45
46
47
48
49
50
51
52
53
54
55
56
57
58
59
60

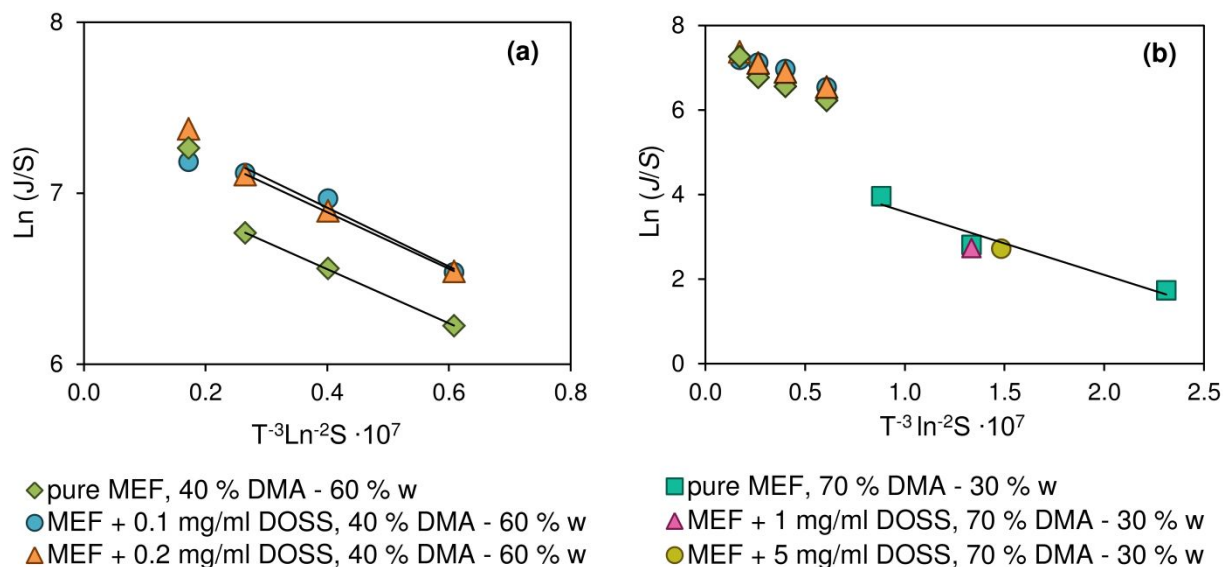


Figure 7 Plot of $\ln(J/S)$ versus $T^{-3} \ln^2 S$ for the determination of the pre-exponential factor A and interfacial energy γ of the nucleation by fitting equation (8), showing (a) data points in 40 % DMA – 60 % water including data in the linear fit at $S^{\text{II}}=2.20-3.30$ and (b) all data points and the fit for pure MEF in 70 % DMA – 30 % water. In 40 % DMA – 60 % water, Form II crystals nucleate and data is plotted using S^{II} , whereas from 70 % DMA – 30 % water Form I crystals are isolated and data is plotted using S^{I} .

Table 5. Pre-exponential factor, A , and the interfacial energy, γ , determined for the nucleation of MEF Form II in 40 % DMA – 60 % water and MEF Form I in 70 % DMA – 30 % water, in the absence or presence of DOSS. In 40 % DMA – 60 % water, fit was determined over $S^{\text{II}}=2.20-4.40$ or $S^{\text{II}}=2.20-3.30$ and as a comparison, A^a and γ^a values obtained using J^a from the fit with LCDF are also included.

	A /m ⁻³ s ⁻¹	γ /mJm ⁻²	R^2	A /m ⁻³ s ⁻¹	γ /mJm ⁻²	R^2	A^a /m ⁻³ s ⁻¹	γ^a /mJm ⁻²	R^{2a}
40 % DMA – 60 % water	S ^{II} =2.20-4.40			S ^{II} =2.20-3.30			S ^{II} =2.20-4.40		
Pure MEF	1800	3.25	0.91	1324	2.92	1.00	742.9	3.03	1.00
MEF + 0.1 mg/mL DOSS	1795	2.87	0.96	2007	3.00	0.98	928.0	3.02	0.99
MEF + 0.2 mg/mL DOSS	2099	3.07	0.99	1904	2.96	1.00	891.8	2.94	1.00
70 % DMA – 30 % water	-			S ^I =1.53-1.99			-		
Pure MEF	-			160	2.86	0.95	-		

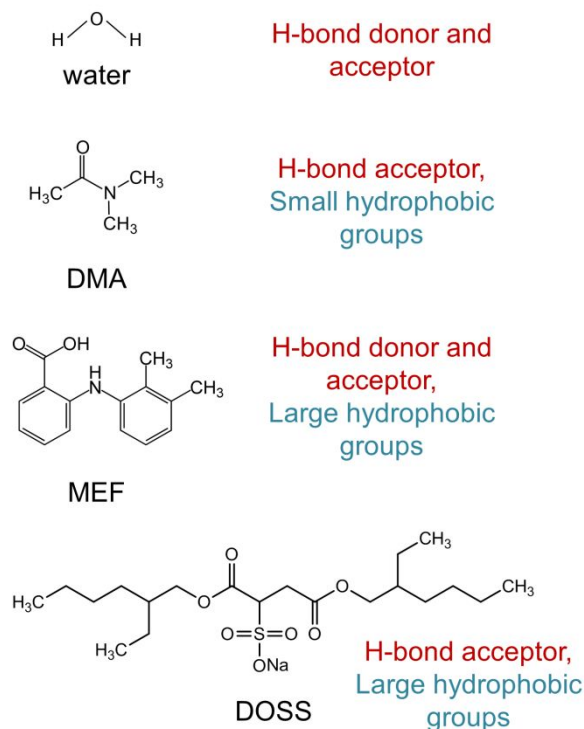
5. DISCUSSION

The main objective of the present work is to investigate how the addition of DOSS influences the nucleation of MEF, and in particular to seek validation of the hypothesis that the reason why DOSS promotes the formation of nanocrystals of MEF in a 5% DMA – 95% water (S approximately in the order of 7000¹⁸) antisolvent process is that DOSS promotes the nucleation of MEF under these conditions. The isothermal antisolvent crystallization protocol employed here, though being laborious, allowed for the rapid creation of uniform supersaturation and investigation of induction times as short as a couple of ten seconds, as opposed to the shortest induction times of ten minutes obtained in the traditional cooling crystallization experiments. The antisolvent experiments were performed at lower DMA content (40 %) and higher supersaturations: $2.20 \leq S^{II} \leq 4.40$, compared to the cooling crystallization experiments at 70 % DMA, and $1.53 \leq S^I \leq 1.99$. In the antisolvent experiments, being closer to the original nanocrystallization conditions¹⁸, the presence of 0.1 mg/mL and 0.2 mg/mL DOSS enhanced the nucleation of MEF crystals by increasing the pre-exponential factor A by approximately 50% (excluding the data points at $S^{II}=4.40$), with no change in the interfacial energy γ .

Within the frame work of the classical nucleation theory, the increase in A in the presence of DOSS, observed in the 40 % DMA – 60 % water mixture, is the result of an increase of the

1
2
3 monomer attachment frequency or in the concentration of nucleation sites (f^*C_0) as the Zeldovich
4 factor, equation (3), does not change since the interfacial energy has been shown to remain
5 essentially unchanged. The attachment frequency parameter, given by equation (4), relates to the
6 rate of transport of molecules to the critical nucleus surface and the likelihood of actually
7 attaching and sticking to the surface. Thus it depends on the diffusion coefficient and the nucleus
8 surface area. The latter remains unchanged if the interfacial energy is uninfluenced. Other
9 parameters remain unchanged (molecular volume, equilibrium solute concentration,
10 supersaturation, temperature) or are as a first approximation assumed to be unchanged (sticking
11 coefficient) with the addition of DOSS in 40 % DMA – 60 % water. The diffusion process
12 describes the transport of the solute molecules from the solution to the surface of the nucleus, and
13 includes desolvation and required conformational changes. Thus, the increase in A in the presence
14 of DOSS may reflect that the transport process is facilitated.

15
16
17
18
19
20
21
22
23
24
25
26
27
28
29
30
31 As shown in Figure 8, the mefenamic acid molecule has hydrogen bond accepting and
32 donating functionalities, but also has large hydrophobic surface patches. In water, the MEF
33 solubility is very low, because the hydrophobic parts of the molecule will force an entropically
34 unfavorable structuring into the surrounding water molecules. The solubility is significantly
35 improved by addition of DMA, but even in 40 % and 70 % by volume DMA – water mixtures the
36 solubility of Form I is only about 0.065 mg/mL (0.27 mmol/L) at 25 °C and 3.8 mg/mL (15.7
37 mmol/L) at 15 °C, respectively.



28 Figure 8 Molecular structure of water, DMA, MEF and DOSS, highlighting the type of
29 functionalities in the molecules.
30
31

32
33 DMA is a polar aprotic solvent having a large dielectric constant and a sizeable dipole
34 moment. The normalized solvent polarity parameter, E_T^N , is 0.38³⁵ and the octanol/water logP
35 value is -0.77³⁶. However, even though DMA and water are fully miscible, the solution is not
36 well mixed on the molecular level³⁷. At DMA in water concentrations of our previous
37 nanocrystallization experiments: 5 % v/v DMA = 1.0 mole %; the tetrahedral structure of normal
38 water predominates in the solution, and the radial distribution function (RDF) reveal the same
39 data as in pure water. At the DMA concentration of the antisolvent nucleation experiments of the
40 present study: 40 % v/v = 11.4 mole %, this water structure starts to disappear, and clusters of
41 DMA molecules begin to form. DMA molecules aggregate with the dipole-dipole interactions
42 between DMA molecules to form DMA clusters stabilized in water by the hydrophobic effect and
43
44
45
46
47
48
49
50
51
52
53
54
55
56
57
58
59
60

1
2
3 by strong hydrogen bonding with water over the carbonyl group. Thus in comparison, the force
4
5 of interaction between DMA molecules is fairly weak. At the conditions of the cooling nucleation
6
7 experiments of the present work: 70 % v/v DMA = 31.1 mole %, the RDF of pure DMA
8
9 gradually dominates. Being an amphiphilic solvent, DMA has hydrophobicity in the methyl
10
11 groups and can thus facilitate the solvation of the hydrophobic parts of MEF, which leads to
12
13 increased solubility. However, in doing so, the DMA molecules partially have to order turning
14
15 the polar side outwards, potentially hydrogen bonding with water. The unfavorable entropy
16
17 decrease in the solvent molecules surrounding the hydrophobic parts of the MEF molecule should
18
19 however be less than in pure water.
20
21
22
23

24 The docusate ion has hydrogen bond accepting functionality that may bond to water and MEF
25
26 but there is no hydrogen bond donating functionality (Figure 8). The docusate ion has a large
27
28 hydrophobic surface, and is expected to more favorably solvate the corresponding MEF
29
30 molecular surface when introduced into the solution, and thus replace the less favorable solvation
31
32 by water and DMA molecules. Hydrophobic interaction is not associated with particular forces
33
34 between MEF and DOSS, and hence because of the weak interaction with DOSS the desolvation
35
36 is facilitated. Accordingly, the attachment frequency factor becomes higher and the nucleation
37
38 becomes facilitated. It appears as if it is more the role of the water that is important, since with
39
40 increasing DMA content from 40 % to 70 %, the favourable effect on the nucleation of adding
41
42 DOSS seems to disappear.
43
44
45
46

47 As mentioned earlier, it has been hypothesized that DOSS promotes the formation of
48
49 nanocrystals of MEF in a 5 % DMA – 95 % water¹⁸. While, unfortunately, we do not have the
50
51 experimental capability to investigate the rate of nucleation at the very high supersaturations in 5
52
53 % DMA, the present work has shown that even at the very much lower supersaturations where
54
55 we are capable of making actual nucleation experiments, a promoting effect can be detected.
56
57
58
59
60

1
2
3 Since the effect was found to relate to the large water content at 40 % DMA and decreases with
4 increasing ratio of DMA in the solvent mixture, it is expected to be even stronger at 5 % DMA,
5 thus supporting the hypothesis that DOSS promotes formation of smaller nanocrystals by
6 increasing the rate of nucleation.
7
8
9
10

11
12 It should be recognized though that in parallel to the increase in DMA content from 5 % to 70
13 %, the supersaturation employed during the crystallization experiments also decreases perhaps
14 even leading to a change from homogeneous to heterogeneous nucleation, and the polymorphic
15 form nucleating possibly changed from the metastable Form II (5 %, 40 % DMA) to the stable
16 Form I (70 % DMA). In addition, while the DOSS concentration employed in 40 % DMA – 60 %
17 water system is only 0.1 - 0.2 mg/mL, the DOSS/MEF molar ratio is 0.14-0.54 (Table 2), which
18 perhaps explains why the results do not show a significant influence of a two fold increase in
19 DOSS concentration.
20
21
22
23
24
25
26
27
28
29

30
31 Without the boundaries of the classical nucleation theory, the situation can be examined from
32 a crystal structure point of view. The two structures of MEF feature the centrosymmetric
33 hydrogen bonded dimerization, and the dimers are basically arranged in stacks linked through C-
34 H... π interactions involving aromatic C-H and the alkylated phenyl ring³⁸. These stacks are then
35 arranged parallel in the crystal structure held together by van der Waals bonding. Presumably, the
36 strongest bonding is the H-bonding between the carboxylic acid groups in the dimers, followed
37 by the bonding between the dimers in the stack. The weakest bonding (per molecule) is likely to
38 be that between the stacks. This agrees with vacuum crystal shape simulations within the
39 Material studio software, using the attachment energy method³⁹. The shape of Form I crystals is
40 plate-like and the axis of the stacks is parallel to the big flat slow growing surface.
41
42
43
44
45
46
47
48
49
50
51
52

53
54 In building the nucleus, we would expect the sequence: dimer formation, stacking and stack
55 binding. In pure water the aggregation of MEF molecules should be significantly influenced by
56
57
58
59
60

1
2
3 hydrophobicity, *i.e.* reducing the exposure of the hydrophobic surfaces of the molecule to water.
4
5 The dimer hydrogen bonding does not contribute to this, and thus dimers should not be expected
6
7 to dominate in the solution. The hydrophobicity will somewhat promote the formation of the
8
9 stacks, but will still leave a significant portion of the hydrophobic surface exposed. The binding
10
11 of the stacks together will reduce the total hydrophobic surface area exposed to water. Adding
12
13 DMA to a water solution will to some extent (as is illustrated by the increase in solubility)
14
15 facilitate the solvation of the hydrophobic parts of MEF, and thus somewhat reduce the
16
17 unfavorable conditions for dimer formation and stacking. Introducing docusate sodium into this
18
19 may further facilitate dimerization and stacking of MEF molecules in the solution, and thus
20
21 promote nucleation.
22
23
24
25

26 In solvating the hydrophobic surface of MEF, DOSS will turn its own hydrophilic hydrogen
27
28 bond accepting surface towards water/DMA. This will reduce the thermodynamically
29
30 unfavorable contact between hydrophobicity and hydrophilicity, and facilitate the formation of
31
32 dimers. If the formation of dimers is facilitated and become the units being transported, addition
33
34 of DOSS will promote the nucleation. As no measurable decrease was observed in the solid-
35
36 liquid interfacial energy at these concentrations of DOSS (Table 5), the governing factor cannot
37
38 be claimed to be improved solvation of the surface of the nucleus by DOSS. In relation to this, it
39
40 is noteworthy that in 40 % DMA – 60 % water, the solubility of MEF in the presence of 0.2
41
42 mg/mL DOSS is essentially unchanged from the value in the absence of DOSS (0.065 ± 0.001
43
44 mg/mL and 0.065 ± 0.003 mg/mL respectively at 25 °C), and in the 70 % DMA – 30 % water
45
46 mixture there is a very slight increase from 3.80 ± 0.01 mg/mL at 15 °C in pure solvent mixture
47
48 to 3.92 ± 0.03 mg/mL in the presence of 5 mg/mL DOSS (Table1).
49
50
51
52

53 Transport and attachment of molecules is required for both the formation of the critical
54
55 nucleus as well as for the growth of the nuclei to detectable size. Accordingly, if the rate of
56
57

molecule attachment is governing, the increase in nucleation rate should correspond to a decrease in time for crystal nuclei to grow to become visible. In fact, in the present work, the growth time t_g is decreased in the presence of DOSS in 40 % DMA – 60 % water over the entire supersaturation range examined. The same relation has been found previously⁴⁰ for *p*-aminobenzoic acid in different solvents, and it was concluded that desolvation of the carboxylic acid group and formation of carboxylic acid dimers is the rate limiting step for nucleation as well as for crystal growth. Studies showing molecular additives to increase the nucleation rate are rather scarce, but it has been found⁴¹ that tailor-made additives can accelerate the growth of γ -glycine along the fast growing pole by disruption of the solvation, and that crystal growth of L-alanine⁴² is accelerated in the presence of L-valine enhancing the rate of surface diffusion.

Another possible mechanism for nucleation rate improvement in the presence of DOSS could be a templating effect of DOSS micelles or single DOSS ions, facilitating the arrangement of MEF molecules to form a nucleus and thus, increasing the pre-exponential factor A . However, in 40 % DMA – 60 % water, micelle formation cannot be detected at the DOSS concentrations employed (Figure S8). In addition, an increasing nucleation promotion effect with increasing DOSS concentration would be expected if DOSS ions acted as nucleation centre which was not found at the concentrations examined here.

6. CONCLUSION

In antisolvent crystallization at 40 % DMA – 60 % water and supersaturations of $S^{II}=4.40$ - 2.20 , DOSS enhanced the nucleation rate of MEF. Within the classical nucleation theory, this increase is due to an increase in the pre-exponential parameter A by 52-44% at 0.1 mg/mL and 0.2 mg/mL DOSS, respectively, while the interfacial energy γ remains essentially unchanged. The analysis leads to the hypothesis that the increase in A is due to an increase in the attachment

1
2
3 frequency of MEF molecules to the growing nucleus, as a result of a facilitated desolvation of
4
5 MEF in the presence of DOSS. This is supported by the fact that also the time of growth to
6
7 visibility t_g is observed to decrease in the presence of DOSS. In the analysis, it is further
8
9 recognised that DOSS may facilitate the formation of MEF dimers, a key element of the crystal
10
11 structure. At 70 % DMA – 30 % water and supersaturations of $S^I=1.99-1.53$, the influence of
12
13 DOSS is very small, suggesting that it is in the presence of higher water concentrations that the
14
15 influence of the surfactant DOSS is more clearly observed.
16
17
18
19
20
21

22 ASSOCIATED CONTENT

23
24
25 **Supporting Information.** Solubility of MEF Form I in 70 % DMA-30% water at different
26
27
28 temperatures (Figure S1); Polymorphic form of MEF crystals nucleated in 40 % DMA – 60 %
29
30 water at $S^{II}=4.40$ (Figure S2) and at $S^{II}=2.20$ (Figure S3) and in 70 % DMA – 30 % at $S^I=1.99$
31
32 (Figure S5); IR spectra showing the timescale of polymorphic transformation in 40 % DMA –
33
34 60 % water (Figure S4); SEM images of Form I crystals obtained as a result of polymorphic
35
36 transformation in 40 % DMA – 60 % water (Figure S6); Determination of nucleation parameters
37
38 in 40 % DMA – 60 % water over the range of $S^{II}=4.40-2.20$ (Figure S7); Figure and discussion
39
40 about the critical micelle concentration of DOSS in different DMA-water mixtures (Figure S8).
41
42
43
44
45
46

47 AUTHOR INFORMATION

48 Corresponding Author

49
50
51 *Email: ake.rasmuson@ul.ie
52
53
54
55
56
57
58
59
60

Notes

The authors declare no competing financial interest.

ACKNOWLEDGMENT

We acknowledge Science Foundation Ireland for the financial support (Grant number: 12/RC/2275). This work was also conducted under the framework of the Irish Government's Programme for Research in Third Level Institutions Cycle 5, with the assistance of the European Regional Development fund.

REFERENCES

- (1) Ku, M. S.; Dulin, W. A biopharmaceutical classification-based Right-First-Time formulation approach to reduce human pharmacokinetic variability and project cycle time from First-In-Human to clinical Proof-Of-Concept. *Pharm. Dev. Technol.* **2012**, *17*, 285–302.
- (2) Gao, L.; Liu, G.; Ma, J.; Wang, X.; Zhou, L.; Li, X. Drug nanocrystals: *In vivo* performances. *J. Control. Release* **2012**, *160*, 418–430.
- (3) Tierney, T. B.; Guo, Y.; Beloshapkin, S.; Rasmuson, Å. C.; Hudson, S. P. Investigation of the particle growth of fenofibrate following antisolvent precipitation and freeze-drying. *Cryst. Growth Des.* **2015**, *15*, 5213–5222.
- (4) Khan, S.; de Matas, M.; Zhang, J.; Anwar, J. Nanocrystal preparation: Low-energy

- precipitation method revisited. *Cryst. Growth Des.* **2013**, *13*, 2766–2777.
- (5) Sun, C. C.; Sun, W.; Price, S.; Hughes, C.; ter Horst, J.; Veessler, S.; Lewtas, K.; Myerson, A.; Pan, H.; Coquerel, G.; van den Ende, J.; Meekes, H.; Mazzotti, M.; Rosbottom, I.; Taulelle, F.; Black, S.; Mackenzie, A.; Janbon, S.; Vekilov, P.; Threlfall, T.; Turner, T.; Back, K.; Cuppen, H.; Toroz, D.; Sefcik, J.; Lovelock, J.; Hammond, R.; Candoni, N.; Simone, E.; Ward, M.; Bertran, C. A.; Vetter, T.; Sear, R.; de Yoreo, J.; Davey, R.; Anwar, J.; Santiso, E.; Wu, D. T.; Roberts, K.; Peters, B.; Schroeder, S.; Rasmuson, A.; Cölfen, H.; Zeglinski, J.; Salvalaglio, M. Solvent and additive interactions as determinants in the nucleation pathway: General discussion. *Faraday Discuss.* **2015**, *179*, 383–420.
- (6) Mochizuki, K.; Qiu, Y.; Molinero, V. Promotion of homogeneous ice nucleation by soluble molecules, *J. Am. Chem. Soc.* **2017**, *139*, 17003–17006.
- (7) Han, G.; Thirunahari, S.; Shan Chow, P.; Tan, R. B. H. Resolving the longstanding riddle of pH-dependent outcome of glycine polymorphic nucleation. *CrystEngComm* **2013**, *15*, 1218–1224.
- (8) Han, G.; Chow, P. S.; Tan, R. B. H. Probing the mechanisms underlying electrolyte-assisted nucleation enhancement of DL-alanine. *Cryst. Growth Des.* **2014**, *14*, 1406–1411.
- (9) Anwar, J.; Boateng, P. K.; Tamaki, R.; Odedra, S. Mode of action and design rules for additives that modulate crystal nucleation. *Angew. Chem. Int. Ed.* **2009**, *48*, 1596–1600.
- (10) Poon, G. G.; Seritan, S.; Peters, B. A design equation for low dosage additives that accelerate nucleation. *Faraday Discuss.* **2015**, *179*, 329–341.
- (11) Poon, G. G.; Peters, B. Accelerated nucleation due to trace additives: A fluctuating coverage model. *J. Phys. Chem. B* **2016**, *120*, 1679–1684.
- (12) Poon, G. G.; Lemke, T.; Peter, C.; Molinero, V.; Peters, B. Soluble oligomeric nucleants: Simulations of chain length, binding strength, and volume fraction effects. *J. Phys. Chem.*

- 1
2
3 *Lett.* **2017**, *8*, 5815–5820.
- 4
5 (13) Pfund, L. Y.; Price, C. P.; Frick, J. J.; Matzger, A. J. Controlling pharmaceutical
6 crystallization with designed polymeric heteronuclei. *J. Am. Chem. Soc.* **2015**, *137*, 871–
7 875.
- 8
9 (14) Verma, V.; Peddapatla, R. V. G.; Crowley, C. M.; Crean, A. M.; Davern, P.; Hudson, S.;
10 Hodnett, B. K. Experimental study on the influence of excipients on the heterogeneous
11 crystallization and dissolution properties of an active pharmaceutical ingredient. *Cryst.*
12 *Growth Des.* **2018**, *18*, 338–350.
- 13
14 (15) Diao, Y.; Whaley, K. E.; Helgeson, M. E.; Woldeyes, M. A.; Doyle, P. S.; Myerson, A. S.;
15 Hatton, T. A.; Trout, B. L. Gel-induced selective crystallization of polymorphs. *J. Am.*
16 *Chem. Soc.* **2012**, *134*, 673–684.
- 17
18 (16) Kim, J.-W.; Park, J.-H.; Shim, H.-M.; Koo, K.-K. Effect of amphiphilic additives on
19 nucleation of hexahydro-1,3,5-trinitro-1,3,5-triazine. *Cryst. Growth Des.* **2013**, *13*, 4688–
20 4694.
- 21
22 (17) Poornachary, S. K.; Han, G.; Kwek, J. W.; Chow, P. S.; Tan, R. B. H. Crystallizing
23 micronized particles of a poorly water-soluble active pharmaceutical ingredient:
24 Nucleation enhancement by polymeric additives. *Cryst. Growth Des.* **2016**, *16*, 749–758.
- 25
26 (18) Bodnar, K.; Hudson, S. P.; Rasmuson, Å. C. Stepwise use of additives for improved
27 control over formation and stability of mefenamic acid nanocrystals produced by
28 antisolvent precipitation. *Cryst. Growth Des.* **2017**, *17*, 454–466.
- 29
30 (19) R. A. Sullivan; Davey, R. J.; Sadiq, G.; Dent, G.; Back, K. R.; Horst, J. H. ter; Toroz, D.;
31 Hammond, R. B. Revealing the roles of desolvation and molecular self-assembly in crystal
32 nucleation from solution: Benzoic and *p*-aminobenzoic acids. *Cryst. Growth Des.* **2014**,
33 *14*, 2689–2696.
- 34
35
36
37
38
39
40
41
42
43
44
45
46
47
48
49
50
51
52
53
54
55
56
57
58
59
60

- 1
2
3 (20) Mealey, D.; Zeglinski, J.; Khamar, D.; Rasmuson, Å. C. Influence of solvent on crystal
4 nucleation of risperidone. *Faraday Discuss.* **2015**, *179*, 309–328.
5
6
7 (21) Jiang, S.; ter Horst, J. H. Crystal nucleation rates from probability distributions of
8 induction times. *Cryst. Growth Des.* **2011**, *11*, 256–261.
9
10
11 (22) Kashchiev, D.; van Rosmalen, G. M. Review: Nucleation in solutions revisited. *Cryst. Res.*
12 *Technol.* **2003**, *38*, 555–574.
13
14
15 (23) Davey, R. J.; Schroeder, S. L. M.; ter Horst, J. H. Nucleation of organic crystals - A
16 molecular perspective. *Angew. Chemie - Int. Ed.* **2013**, *52*, 2166–2179.
17
18
19 (24) Brandel, C.; Horst, J. H. Measuring induction times and crystal nucleation rates. *Faraday*
20 *Discuss.* **2015**, *44*, 199–214.
21
22
23 (25) Gilpin, R. K.; Zhou, W. Infrared studies of the thermal conversion of mefenamic acid
24 between polymorphic states. *Vib. Spectrosc.* **2005**, *37*, 53–59.
25
26
27 (26) Romero, S.; Escalera, B.; Bustamante, P. Solubility behavior of polymorphs I and II of
28 mefenamic acid in solvent mixtures. *Int. J. Pharm.* **1999**, *178*, 193–202.
29
30
31 (27) Jabeen, S.; Dines, T. J.; Leharne, S. A.; Chowdhry, B. Z. Raman and IR spectroscopic
32 studies of fenamates - Conformational differences in polymorphs of flufenamic acid,
33 mefenamic acid and tolfenamic acid. *Spectrochim. Acta Part A Mol. Biomol. Spectrosc.*
34 **2012**, *96*, 972–985.
35
36
37 (28) Maggioni, G. M.; Mazzotti, M. Stochasticity in primary nucleation: Measuring and
38 modeling detection times. *Cryst. Growth Des.* **2017**, *17*, 3625–3635.
39
40
41 (29) Maggioni, G. M.; Mazzotti, M. Modelling the stochastic behaviour of primary nucleatio.
42 *Faraday Discuss.* **2015**, *179*, 359–382.
43
44
45 (30) Xiao, Y.; Tang, S. K.; Hao, H.; Davey, R. J.; Vetter, T. Quantifying the inherent
46 uncertainty associated with nucleation rates estimated from induction time data measured
47
48
49
50
51
52
53
54
55
56
57
58
59
60

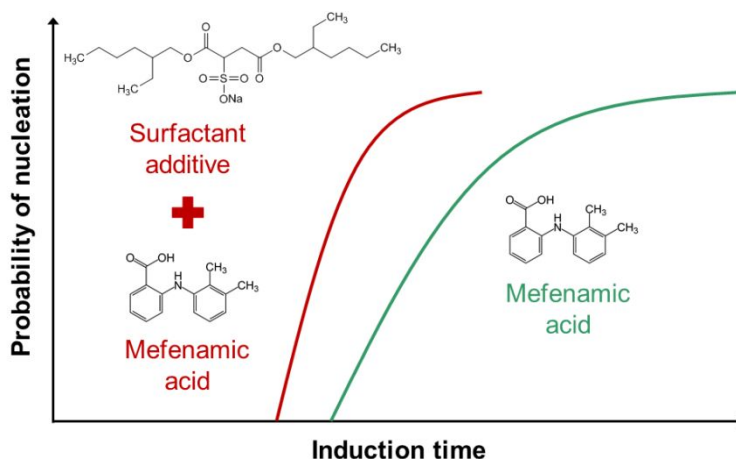
- 1
2
3 in small volumes. *Cryst. Growth Des.* **2017**, *17*, 2852–2863.
4
5
6 (31) Maggioni, G. M.; Bosetti, L.; dos Santos, E.; Mazzotti, M. Statistical analysis of series of
7
8 detection time measurements for the estimation of nucleation rates. *Cryst. Growth Des.*
9
10 **2017**, *17*, 5488–5498.
11
12 (32) Kadam, S. S.; Kulkarni, S. A.; Coloma Ribera, R.; Stankiewicz, A. I.; ter Horst, J. H.;
13
14 Kramer, H. J. M. A new view on the metastable zone width during cooling crystallization.
15
16 *Chem. Eng. Sci.* **2012**, *72*, 10–19.
17
18 (33) Mealey, D.; Croker, D. M.; Rasmuson, Å. C. Crystal nucleation of salicylic acid in organic
19
20 solvents. *CrystEngComm* **2015**, *17*, 3961–3973.
21
22 (34) Zeglinski, J.; Kuhs, M.; Khamar, D.; Hegarty, A. C.; Devi, R. K.; Rasmuson, Å. C. Crystal
23
24 nucleation of tolbutamide in solution: Relationship to solvent, solute conformation, and
25
26 solution structure. *Chem. - Eur. J.* **2018**, *24*, 4916–4926.
27
28 (35) Reichardt, C. *Solvents and solvent effects in organic chemistry*; WILEY-VCH Verlag
29
30 GmbH & Co. KGaA: Weinheim, 2003.
31
32 (36) Smallwood, I. M. *Handbook of organic solvent properties*; Arnold (London) & Halsted
33
34 Press (New York), 1996.
35
36 (37) Takamuku, T.; Matsuo, D.; Tabata, M.; Toshio Yamaguchi; Nishi, N. Structure of aqueous
37
38 mixtures of *N,N*-dimethylacetamide studied by infrared spectroscopy, X-ray diffraction,
39
40 and mass spectrometry *J. Phys. Chem. B* **2003**, *107*, 6070–6078.
41
42 (38) Seethalekshmi, S.; Row, T. N. G. Conformational polymorphism in a non-steroidal anti-
43
44 inflammatory drug, mefenamic acid. *Cryst. Growth Des.* **2012**, *12*, 4283–4289.
45
46 (39) Waknis, V.; Chu, E.; Schlam, R.; Sidorenko, A.; Badawy, S.; Yin, S.; Narang, A. S.
47
48 Molecular basis of crystal morphology-dependent adhesion behavior of mefenamic acid
49
50 during tableting. *Pharm. Res.* **2014**, *31*, 160–172.
51
52
53
54
55
56
57
58
59
60

- 1
2
3 (40) Davey, R. J.; Back, K. R.; Sullivan, R. A. Crystal nucleation from solutions – Transition
4 states, rate determining steps and complexity. *Faraday Discuss.* **2015**, *179*, 9–26.
5
6
7 (41) Dowling, R.; Davey, R. J.; Curtis, R. A.; Han, G.; Poornachary, S. K.; Chow, P. S.; Tan,
8 R. B. H. Acceleration of crystal growth rates: An unexpected effect of tailor-made
9 additives. *Chem. Commun.* **2010**, *46*, 5924–5926.
10
11
12 (42) Yang, X.; Qian, G.; Duan, X.; Zhou, X. Impurity effect of L-valine on L-alanine crystal
13 growth. *Cryst. Growth Des.* **2013**, *13*, 1295–1300.
14
15
16
17
18

19 For Table of Contents (TOC) use only

20 Promotion of Mefenamic Acid Nucleation by a Surfactant Additive, Docusate Sodium

21
22
23
24
25 *Katalin Bodnár, Sarah P. Hudson, Åke C. Rasmuson*
26
27
28
29



45 Synopses

46
47
48 Nucleation of mefenamic acid in the presence of an anionic additive, docusate sodium was
49 enhanced in 40 % water - 60 % DMA mixture.
50
51
52
53
54
55
56
57